Macromolecules
ARTICLE

Macromolecules **2010**, *43*, 3383–3391 **3383**
DOI: 10.1021/ma9026178

Association Strength of Metal Ions with Poly(4-vinylpyridine) in Inorganic/Poly(4-vinylpyridine)-*b*-poly(ε-caprolactone) Hybrids

Tao Lin,[†] Chien-Lin Li,[‡] Rong-Ming Ho,*[,†,‡] and Jia-Chong Ho[§]

[†]*Institute of Nanoengineering and Microsystems, Nationsal Tsing-Hua University, Hsinchu 30013, Taiwan,* [‡]*Department of Chemical Engineering, Nationsal Tsing-Hua University, Hsinchu 30013, Taiwan, and* [§]*Electronics Research & Service Organizations, Industrial Technology Research Institute, Hsinchu 30013, Taiwan*

Received November 27, 2009; Revised Manuscript Received March 1, 2010

ABSTRACT: A series of inorganic/poly(4-vinylpyridine)-*b*-poly(ε-caprolactone) (P4VP−PCL) hybrids were prepared to examine the phase behavior of hybridization. Various metal ions including Au^{3+}, Cu^{2+}, Cu^{+}, and Ag^{+} ions were used for the hybridization. As demonstrated by transmission electron microscopy, the phase transformation of self-assembled nanostructures can be easily induced by adding small amount of metal ions due to the association of metal ions with P4VP block that profoundly creates the extra volume in P4VP microdomain (i.e., gives rise to the significant increase of effective excluded volume) beside the Ag^{+} ions. The variation in the effective excluded volume (relevant to the degree of domain swelling, as evidenced by small-angle X-ray scattering) is strongly dependent upon the association strength of the metal ions with the P4VP block, as determined by Fourier transform infrared spectroscopy. The association strength for the formation of the hybrids follows the order of $Au^{3+} > Cu^{2+}$ and $Cu^{+} > Ag^{+}$. Accordingly, the degree of domain swelling in the hybrids increases with the enhancement of association strength following the order of $Au^{3+} > Cu^{2+}$ and $Cu^{+} > Ag^{+}$. Furthermore, as demonstrated in the hybrids of Au nanoparticles and P4VP−PCL, a dramatic decrease of the association strength can be found in the hybrids after reduction. Consistent with the theoretical prediction, the reduction of metal ions causes the alleviation of the association strength. The association effect is also dependent upon the particle size; the larger the particle size is, the weaker the association will be. Consequently, the accommodation of the metal nanoparticles within the P4VP microdomain is justified by the size of the metal nanoparticles.

Introduction

The hybrids comprising of inorganic and organic materials have attracted intensive attention in the past decade because of their tremendous potentials in applications by combining inorganic and organic characters for functions and complexity. Additionally, the hybridization of inorganic and organic materials provides a great versatility and easy fabrication for the demands of modern materials by combining important properties into a single composition system through tuning and tailoring of functionalities. In addition to the useful properties of inorganic materials such as excellent mechanical property, thermal conductivity, and electrical conductivity, novel properties due to the quantum-size effect have been exploited by academia and industries. To fabricate the nanostructures for the inorganic materials, the self-assembly of block copolymers (BCPs) becomes one of the best approaches to serve as organic templates to attract, separate, and arrange the inorganic materials in nanoscale. Although the combination of inorganic materials and BCPs has given rise to a great diversity of applied materials[1−13] such as metal−organic frameworks[12] and ionic liquid-BCPs composites,[13] the phase behavior of inorganic/BCP hybrids is still not well-understood. As a result, it is important to realize the corresponding phase behavior with regard to the control of hybridized nanostructures for functions and complexity.

Recently, Ginzburg, Balazs, and co-workers used both systematic simulations and theoretical study to describe the phase behavior of the nanoparticles (NPs)/BCP hybrids. They predicted that the size and the amount of inorganic NPs can be exploited to control the phase behavior of NPs/BCP hybrids.[14] Both simulated and theoretical phase diagrams revealed that phase transformation can be induced by the introduction of NPs. Interestingly, the simulated phase diagrams of NPs/BCP hybrids qualitatively agreed with the results for the phase behavior of homopolymer/BCP blends[15] and selective solvent/BCP mixtures[16] at which the low-molecular-weight homopolymers and selective solvent in the blends presumably act much like small NPs in the hybrids. Moreover, an increase in the volume fraction of the NPs would give rise to the swelling of the phase-separated hybridized microdomains.[17] Through the control of the NPs size, the appearance of new self-assembled morphologies including the morphologies of center-packing and edged-packing NPs have been also predicted.[18]

To examine the phase behavior of NPs/BCP hybrids, a convenient method is to modify the surface properties of insoluble inorganic NPs by ex-situ presynthesis and surface modification for hybridization. Such an approach makes it easy to control the size of inorganic NPs so as to define the dispersion of NPs.[10,19,20] Although this ex-situ hybridization takes advantage of the chemically attractive interaction between the BCP and the functionalized NP surface so as to allocate the nanoparticles in the hybrids precisely, this approach is difficult to describe the real phase behavior of inorganic/BCPs hybrids at which the association is caused by the BCP and organic ligands used for modifying the surface of nanoparticle. In contrast, in situ hybridization by directly hybridizing inorganic precursors and BCPs can be used

*To whom correspondence should be addressed: Tel 886-3-5738349; Fax 886-3-5715408; e-mail rmho@mx.nthu.edu.tw.

Published on Web 03/10/2010

Table 1. Characterization of P4VP−PCL BCPs

sample	M_n^{P4VP} (g/mol)[a]	M_n^{PCL} (g/mol)[a]	M_n^{total} (g/mol)	f_{P4VP}	PDI[b]	morphology
V2C7	2000	7000	9000	0.24	1.25	cylinder
V4C7	4000	7000	11000	0.38	1.24	cylinder
V3C5	2900	5400	8300	0.37	1.25	cylinder
V15C5	15000	5400	20400	0.75	1.28	cylinder
V22C5	21600	5400	27000	0.81	1.29	cylinder

[a] M_n^{P4VP} and M_n^{PCL} were characterized by proton nuclear magnetic resonance (^{1}H NMR). [b] The polydispersity index (PDI) in the diblock copolymers was determined by GPC using standard calibration.

to resolve these difficulties.[2,21−30] Through the hydrogen bonding and dipole−dipole interaction between the poly(ethylene oxide) block and metal alkoxides, Wiesner and co-workers examined the phase transformation of inorganic/BCP hybrids by directly mixing the metal alkoxides into the poly(isoprene-*block*-(ethylene oxide)) (PI−PEO).[2] Furthermore, the preparation of ionic conductors by Bates and co-workers indicated that the original phase behavior of poly((styrene)-*block*-isoprene-*block*-ethylene oxide) (PS−PI−PEO) can be smoothly modified by doping lithium perchlorate.[21] Selective mixing of this salt with the PEO blocks significantly enhanced the order−disorder transition temperature and expanded the ordered microdomain lattices. Through the metalation of various gold ions (it includes neutral gold salt ($NaAuCl_4$) and strong-protonated gold salt ($HAuCl_4$)) with the poly(ethylene oxide-*block*-(4-vinylpyridine)) (PEO−P4VP), Eisenberg, Sidorov, Bronstein, and co-workers demonstrated that the micellization of PEO−P4VP BCPs can be affected by adjusting the association strength of the metal ions with the P4VP block.[22] Kim and co-workers examined the domain variation of $CdCl_2$/PS−P2VP and $CdCl_2$/PS−P4VP hybrids, suggesting that intramolecular and intermolecular coordination can be formed by association of Cd^{2+} with the P2VP and P4VP block, respectively, so as to cause morphological evolution.[23,24] Lodge and co-workers combined the ionic liquid and poly((butadiene-*block*-ethylene oxide) (PB−PEO) to form ionic gels with practical applications.[25,26] Furthermore, through the identification of disorder to order transition (DOT) in lithium salts/poly-((styrene)-*block*-methyl methacrylate) (PS−PMMA) hybrids, Russell and co-workers suggested that the overall segmental interaction, especially for entropic part, is significantly increased as a result of ionic complex formation.[27,28] Our previous results in the Au^{3+}/P4VP−PCL hybrids indicated that interesting morphological evolution can be observed at which the introduction of gold precursors was preferentially associated with the P4VP microdomain and thus induced the phase transformation from cylinder phase to lamellar phase.[29] Also, the PCL block of the P4VP−PCL BCPs plays an important role to stabilize the phase behavior of hybrids so as to prevent the occurrence of disorder nanostructures during hybridization.[30]

To generalize the phase behavior of metal species/P4VP−PCL hybrids, various metal ions including Au^{3+}, Cu^{2+}, Cu^{+}, and Ag^{+} ions are introduced into the P4VP−PCL BCPs for hybridization in this study. We aim to examine the association mechanisms of the variety of metal ions with the pyridine in the P4VP block so as to realize the corresponding association effects on the phase behavior of the hybrids, in particular the phase transformation behavior due to the effective excluded volume resulting from domain swelling. The association strength of the metal ions with the P4VP block can be determined by Fourier transform infrared spectrum (FTIR) so as to correlate the degree of domain swelling determined by small-angle X-ray scattering (SAXS). The association strength for the formation of the hybrids follows the order of $Au^{3+} > Cu^{2+}$ and $Cu^{+} > Ag^{+}$ so as for the degree of domain swelling. Furthermore, a dramatic decrease of the association strength can be found in the hybrids after the reduction of the metal ions, as demonstrated in the hybrids of Au NPs and P4VP−PCL BCPs. Through the well control of metal ion reduction (i.e., NP formation) by in situ liquid−gas interfacial reduction, the particle size effect on the association strength can be justified by the accommodation of the metal nanoparticles within the P4VP microdomain; the larger the particle size is, the weaker the association will be.

Experimental Section

Materials. A series of P4VP−PCL BCPs were synthesized via living ring-opening and atom transfer radical polymerizations in sequence. The molecular characteristics and the sample codes of the P4VP−PCL BCPs are described in Table 1. Hydrogen tetrachloroaurate(III) trihydrate ($HAuCl_4 \cdot 3H_2O$) was purchased from Alfa Aesar (Ward Hill, MA). Silver nitrate crystal ($AgNO_3$) was purchased from Mallinckrodt Chemicals (Phillipsburg, NJ). Copper(I) acetate (CuAc) and copper(II) acetate hydrate ($Cu(Ac)_2 \cdot xH_2O$) were purchased from Aldrich (St. Louis, MO).

Nanostructures of P4VP−PCL BCPs. Bulk samples of P4VP−PCL BCPs were prepared by the solutions-casting method using dichloromethane (CH_2Cl_2) solutions (10 wt % of P4VP−PCL) at room temperature. To eliminate possible effects of PCL crystallization and residual solvent on microphase-separated morphology during solvent evaporation, we annealed all bulk samples at 140 °C, which is above the glass transition temperature of P4VP block ($T_{g,P4VP} \sim 100$ °C) and well above the equilibrium melting point ($T_m^{\circ}{}_{,PCL} = 69$ °C) of PCL block but below estimated order−disorder transition temperature ($T_{ODT} \sim 230$ °C), for 12 h under a nitrogen atmosphere. After thermal treatment, the samples were rapidly cooled at a rate of 150 °C/min to room temperature. Subsequently, the samples were examined by both TEM and SAXS experiments.[30]

Metal Ions/P4VP−PCL Hybridization. Hydrogen tetrachloroaurate(III) trihydrate ($HAuCl_4 \cdot 3H_2O$), silver nitrate crystal ($AgNO_3$), copper(I) acetate (CuAc), and copper(II) acetate hydrate ($Cu(Ac)_2 \cdot xH_2O$) were used as inorganic species to associate with the P4VP−PCL BCPs for the formation of hybridized materials. By taking advantage of the association between the nitrogen lone-pair electrons of the pyridine and various metal ions, the hybridization can be simply achieved by solution mixing using dichloromethane (CH_2Cl_2) solution (1 wt % gold/P4VP−PCL) with specific ratio of nitrogen on P4VP block to metal ions (M^{n+}/N). The solution was then stirred for 1 day to allow complete solubilization of the various metal ions. The bulk samples of various metal ions/P4VP−PCL hybrids were prepared by casting from the prepared solutions. The cast samples were then thermally treated following a similar procedure for neat BCP samples previously described. The added amount of the gold precursors was defined by the stoichiometry of the M^{n+}/N ratio to determine the degree of association. In our previous study, the phase behavior of the Au^{3+}/P4VP−PCL hybrids can be effectively affected by the association of the metal ions with the P4VP block so as to induce the phase distortion and transformation.[29,30] To realize this unexpected morphological evolution, a relatively small amount of metal ions (M^{n+}/N = 1/10, 1/20) are used in this study for hybridization.

Reduction. To examine the morphological variation from Au^{3+} ions to Au NPs, polymer solution with gold precursors (1 wt %) was transferred to a vial for the reduction of the gold precursors. For liquid−vapor interfacial reduction, the

aluminum holder filled with hydrazine liquid was fixed on the inner wall of the vial so as to carry out the liquid−vapor interfacial reaction from the polymer solution and hydrazine vapor. The color of the polymer solution was changed from yellow to dark purple after reduction, suggesting the formation of Au NPs. For solid−liquid interfacial reduction, a flake of hybridized sample sliced from a bulk sample was immersed into the hydrazine liquid to carry out the solid−liquid interfacial reaction. After reduction, the outer region of the flake appeared as dark purple color, indicating the formation of Au NPs.

Density Measurement. After long time annealing to release the bubbles trapped in bulk samples, the densities of the hybrids were measured by a hydrometer using various aqueous NaCl solutions with different NaCl concentrations as standards.

Instrumental Details. Differential scanning calorimetry (DSC) experiments were carried out in a Perkin-Elmer DSC 7 equipped with an intracooler and calibrated with cyclohexane and indium for the measurements of thermal behavior of P4VP−PCL. Bright field transmission electron microscopy (TEM) images were obtained using the mass−thickness contrast with a JEOL TEM-1200x transmission electron microscope (at an accelerating voltage of 120 kV). Ultrathin sectioning (50−60 nm) was performed by ultramicrotomy (LEICA ULTRACUT R) with cooling system (LEICA EMFCS) at −100 °C. Staining was accomplished by exposing the samples to the vapor of a 4% aqueous RuO4 solutions for 30 min. SAXS experiments ($\log(q)$ vs q ($= 4\pi \sin(\theta/2)/\lambda$); here, q is the scattering vector and θ is the scattering angle) were conducted at the beamline BL17B3 of the Nationsal Synchrotron Radiations Research Center (NSRRC). The incident X-ray beam was focused vertically by a mirror and monochromated to the energy of 10 keV by a germanium (111) double-crystal monochromator. The wavelength of the X-ray beam was 1.24 Å. The beam stop was a round tantalum disk 4 mm in diameter. A MAR CCD X-ray detector (MAR USA) was used to collect the two-dimensionsal (2D) SAXS patterns. The scattering angle of the SAXS pattern was calibrated using silver behenate. To eliminate the disturbance of crystallization, all samples were heated over 70 °C (the melting point of PCL segment is about 55 °C). FTIR experiments were collected on a Bomem, DA8.3 spectrometer at a resolution of 1 cm^{-1}. The films for FTIR measurements were prepared by casting solution onto 1 cm × 1 cm silcon wafer (100) and dried to prevent the disturbance of water. The experiments were carried out at room temperature (25 °C).

Results and Discussion

Phase Behavior of Various Metal Ions/P4VP−PCL Hybrids. Figure 1a shows 1D SAXS profiles of the V2C7 ($f_{P4VP}{}^{v} = 0.24$) at which the scattering peaks occur at the q^* ratios of 1:2:$\sqrt{7}$, suggesting a cylinder phase. The cylinder phase can be further confirmed by TEM observation at which the dark region represents the P4VP microdomain and the bright region is the PCL microdomain due to RuO_4 staining (Figure S1 of Supporting Information). For hybridization, various metal ions including Au^{3+} from $HAuCl_4$, Cu^{2+} from $Cu(Ac)_2$, Cu^+ from CuAc, and Ag^+ from $AgNO_3$ were introduced into the V2C7. Similar to the SAXS results of the V2C7, the Au^{3+}/V2C7, Cu^{2+}/V2C7, and Cu^+/V2C7 hybrids appear as cylinder phase by introducing small amount of metal ions (as illustrated in Figure 1b−d for the hybrids at a hybrid ratio of 1/20). The corresponding TEM images of the hybrids further confirm the appearance of well-defined cylindrical morphologies (Figure 1f−h). Also, no significant aggregation of the metal ions can be found in those hybrids such that suggests the uniform dispersion of introduced Au^{3+}, Cu^{2+}, and Cu^+ ions in the P4VP microdomains through the association of metal ions with the lone pair electron of nitrogen in the P4VP block. Accordingly, those hybrids appear as homogeneous hybrids. By contrast,

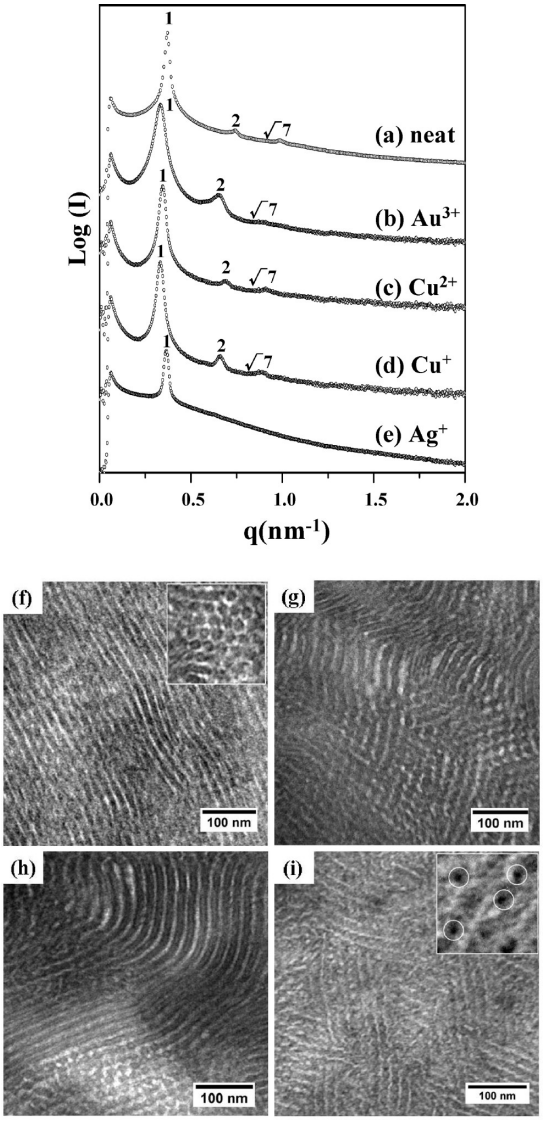

Figure 1. 1D SAXS profiles of (a) V2C7 ($f_{P4VP}{}^{v} = 0.24$) and its hybrids with (b) $HAuCl_4$, (c) $Cu(Ac)_2$, (d) CuAc, (e) $AgNO_3$ at a hybrid ratio of 1/20. Corresponding TEM micrographs of the hybrids with (f) $HAuCl_4$, (g) $Cu(Ac)_2$, (h) CuAc, and (i) $AgNO_3$. The micrograph in the inset of (f) shows the top view of the cylinders, and the micrograph in the inset of (i) shows the enlarged image at which the silver aggregates are marked by the white circles. All samples are stained by RuO_4 at which the dark region represents the P4VP microdomain and the bright region is the PCL microdomain.

only primary peak can be recognized in the Ag^+/V2C7 hybrids (Figure 1e). The corresponding TEM results show the expected cylindrical morphology (Figure 1i). Nevertheless, the aggregation of silver precursors with size ~5 nm can be clearly identified as marked by the white circles in the enlarged image in the inset of Figure 1i. Conversely, the amount of silver ions associated with P4VP blocks may reach a limit so as to cause the aggregation near the P4VP microdomains from exclusion (see below for reason). Owing to the strong scattering from the aggregates of silver ions, the scattering results from hexagonally packed cylinders might be concealed. Apart from the scattering effect caused by the aggregates of silver ions, the fluctuation at the microdomain interfaces (Figure 1i) might be one of the reasons to cause the absence of higher order reflections in SAXS profile. Nevertheless, a significant contribution of Ag scattering can be observed in the hybrids with higher concentration of the Ag^+

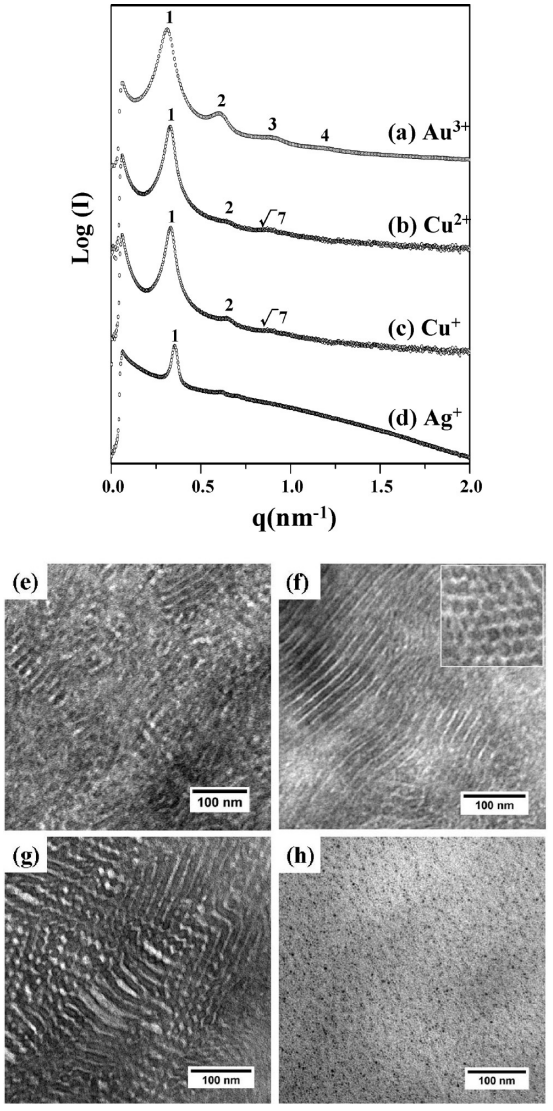

Figure 2. 1D SAXS profiles of V2C7 (f_{P4VP}^{v} = 0.24) hybrids with (a) $HAuCl_4$, (b) $Cu(Ac)_2$, (c) CuAc, and (d) $AgNO_3$ at a hybrid ratio of 1/10. Corresponding TEM micrographs of the hybrids with (e) $HAuCl_4$, (f) $Cu(Ac)_2$, (g) CuAc, and (h) $AgNO_3$. The micrograph in the inset of (f) shows the top view of the cylinders. All samples are stained by RuO_4 at which the dark region represents the P4VP microdomain and the bright region is the PCL microdomains.

ions (Ag^+/P4VP = 1/7). As a result, we suggest that the scattering effect is mainly attributed to the cause of the aggregation scattering.

Notably, the primary peak of the hybrids slightly shifts to lower value with the addition of small amount of metal ions, especially in the homogeneous hybrids. The results indicate that the interdomain spacing of the microphase-separated microdomain increases with the addition of metal ions. It is in line with the behavior of effective excluded volume as observed previously;[30] the introduced metal ions strongly affect the surrounding P4VP chains to lead the significant increase in excluded volume.

The apparent excluded volume is thus defined as effective excluded volume from hybridization. Consequently, instead of simple swelling by the intrinsic volume of the metal ions, the association of the metal ions and the lone pair of the nitrogen in the P4VP block profoundly creates extra volume in the P4VP microdomain. As a result, a phase transformation from the cylinder phase to lamellar phase is expected by

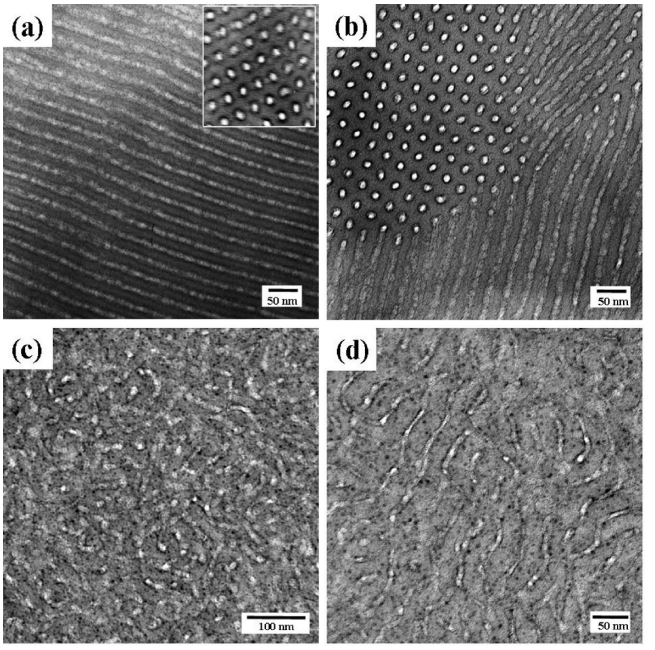

Figure 3. TEM micrographs of (a) V15C5 (f_{P4VP}^{v} = 0.75) sample, (b) V22C5 (f_{P4VP}^{v} = 0.81) sample, (c) Ag^+/V15C5 hybrid, and (d) Ag^+/V22C5 hybrid at a hybrid ratio of 1/7. The micrograph in the inset of (a) shows the top view of the cylinders. All samples are stained by RuO_4 at which the dark region represents the P4VP microdomain and the bright region is the PCL microdomain.

introducing a larger amount of the Au^{3+} ions. As illustrated in Figure 2e, the hybrid at a hybrid ratio of 1/10 appears as a lamellar phase. The corresponding SAXS results further confirm the observed morphology at which the reflections at the q^* ratios of 1:2:3:4 can be identified (Figure 2a). By contrast, instead of the phase transformation, the microphase-separated morphologies in the Cu^{2+}/V2C7 and Cu^+/V2C7 hybrids remain as cylinder phase at the same hybrid ratio of 1/10, as evidenced by SAXS (Figure 2b,c) and TEM (Figure 2f,g) results, respectively. As a result, we conjecture that the association strength of the Cu^{2+} and the Cu^+ ions with the P4VP block should be weaker than that of the Au^{3+} ions (see below for reasons). In the Ag^+/V2C7 hybrids, by increasing the hybrid ratio from 1/20 to 1/10, significant aggregation can be found, as evidenced by TEM observation (Figure 2h). A primary peak with invariant peak position as the V2C7 can be identified in the SAXS result (Figure 2d). Accordingly, the association strength between the Ag^+ ions and the P4VP block should be trivial so that the exclusion of supersaturated Ag^+ ions would easily occur. In contrast to the P4VP−PCL BCPs with short P4VP chain, it is reasonable to conjecture that a large amount of the metal ions can be associated with the P4VP block by increasing the P4VP chain length in the P4VP−PCL BCPs. To further examine the phase behavior of the hybrids, the P4VP−PCL BCPs with longer P4VP chain, such as V22C5 (f_{P4VP}^{v} = 0.81) and V15C5 (f_{P4VP}^{v} = 0.75), were used for hybridization.

The intrinsic morphologies of V15C5 and V22C5 are cylinders as shown in Figure 3a,b. In the hybrids with the Au^{3+} ions at a hybrid ratio of 1/7, no significant microphase separation was found, suggesting that the self-assembly of the P4VP−PCL BCPs is entirely interrupted by the strong association between the Au^{3+} ions and the P4VP block.

It is consistent with our previous results;[30] for the P4VP-rich P4VP−PCL hybrids, the bridging for hybridized P4VP chains can be effectively achieved. As a result, the driving force for bridging resulting from the strong association of the

Au^{3+} ions, and the P4VP block inhibits the formation of ordered nanostructures. To moderate this unexpected interruption from hybridization, the Au^{3+} ions were replaced by the Ag^{+} ions so as to reduce the association strength of metal ions with the P4VP block. Owing to the weak association, the TEM images of Ag^{+}/V15C5 and Ag^{+}/V22C5 hybrids reveal intrinsic cylindrical morphologies as shown in Figure 3c,d, but significant Ag^{+} aggregation besides slight domain swelling can be found. By comparing the morphologies of neat samples (Figure 3a,b) with that of hybrids (Figure 3c,d), it reveals that only a small amount of Ag^{+} ions can be stabilized in the P4VP microdomain due to the weak association. As a result, the driving force from the hybridization is not strong enough to drive the occurrence of phase transformation from cylinder to sphere phase; instead, it would cause the distortion of nanostructures resulting from domain swelling.

On the basis of the morphological observations, it reflects that the phase behavior of the metal ions/P4VP−PCL hybrids can be justified by introducing various metal ions. Notably, the phase behavior of metal ions/BCP hybrids is very different than the phase behavior of homopolymer/BCP blends. In the homopolymer/BCP system, the volume fraction of final blends can be precisely calculated by the added volume of homopolymer.[15] By contrast, phase transformation in the metal ions/BCP hybrids can be found by adding a small amount of metal ions due to the significant increase in excluded volume.[30] The variation is attributed to the distinct association behavior at which the associations in the metal ions/BCP hybrids and homopolymer/BCP blends are metal−polymer ligand coordination and van der Waals interactions, respectively. The binding energy (i.e., association strength) of metal−polymer ligand coordination is several times higher than that of van der Waals force, suggesting that higher chain stretching is expected to be caused by the metal−polymer ligand coordination. We thus infer that the association strength of metal ions with P4VP block may play a critical role to determine the final morphology of the hybrids. To further examine the association strength for various metal ions/P4VP−PCL hybrids, FTIR experiments were carried out.

Association Strength of Various Metal Ions with P4VP Block. Figure 4a shows the FTIR spectrum of the V2C7 at which the absorption peak at 1597 cm^{-1}, corresponding to the characteristic CN stretching vibration of pyridine, can be identified. In the Au^{3+}/V2C7 hybrid (Figure 4b), in addition to the CN characteristic absorption peak, a new absorption peak at 1635 cm^{-1} can be found.

We suggest that the significant blue shift of the CN stretching vibration is attributed to the association of metal ions with the lone pair nitrogen in the P4VP block so as to cause the change of the in-plane CN stretching vibration mode (that is, the increase of binding energy associated with in-plane CN stretching). Similar results have been found by Belfiore and co-workers; they demonstrated that the association of Ru^{2+} ions with the P4VP exhibits a significant blue shift (approximately 15−20 wavenumbers) in FTIR spectra due to the formation of metal−ligand π-bonding for the pyridine group.[31] As a result, the degree of the blue shift can be used as an indicator to determine the association strength of the metal ions with the P4VP block.

A new absorption at 1614 cm^{-1} can be identified in the Cu^{+}/V2C7 and Cu^{2+}/V2C7 hybrids (Figure 4c,d). Note that the blue shift of the CN characteristic absorption peak in the hybrids with the copper ions is smaller than that with the Au^{3+} ions. Consistent with the remarks from the morphological observations, the results suggest that the association

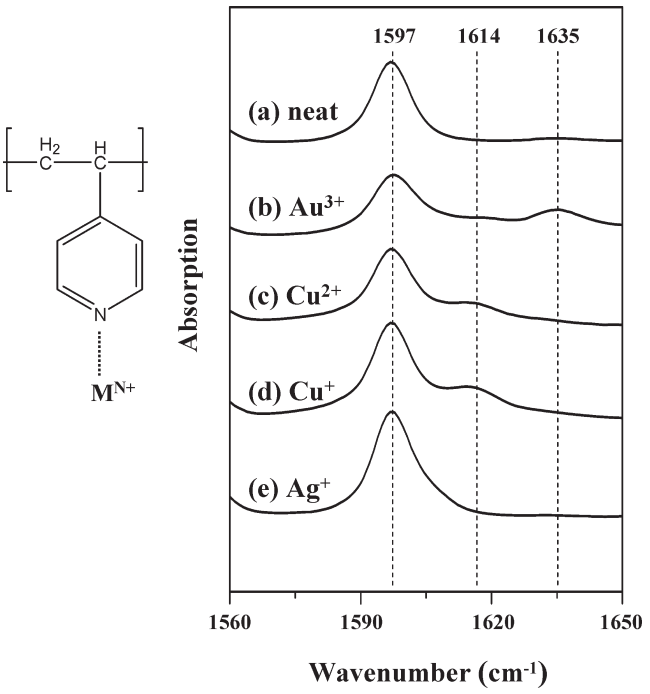

Figure 4. FTIR spectra of (a) V2C7 (f_{P4VP}^{v} = 0.24) and its hybrids with (b) $HAuCl_4$, (c) $Cu(Ac)_2$, (d) CuAc, and (e) $AgNO_3$ at a hybrid ratio of 1/20.

strength of the Cu^{+} and the Cu^{2+} ions with the P4VP block is indeed lower than the Au^{3+} ions. The discrepancy between the association strength of the gold and copper ions with the P4VP block resulted from the variation in association mode. In the hybrids with the gold ions, the pyridine ring can be converted to positively charged pyridine ring due to the protonation by the acidic gold precursor. By contrast, in the hybrids with the copper ions, the association is simply attributed to the coordination (that is, the nominal complexation of the pyridine ring with the copper precursor). Consequently, in the Ag^{+}/V2C7 hybrids, it is reasonable to infer that the blue shift should be insignificant due to the weak complexation between the Ag^{+} ions and the P4VP. As shown in Figure 4e, no new absorption can be recognized in the Ag^{+}/V2C7 hybrids.

Domain Swelling in Various Metal Ions/P4VP−PCL Hybrids. As observed, the introduction of the metal ions in the P4VP−PCL BCPs may give rise to the significant swelling of microphase-separated P4VP microdomain due to the association of the metal ions with the P4VP block. We conjecture that the degree of swelling (namely, the contribution of effective excluded volume) would be dependent upon the association strength of the metal ions with the P4VP block. To further examine the swelling behavior of P4VP microdomain after hybridization, the primary peaks of the SAXS profiles in Figures 1 and 2 are summarized in Table 2. Note that there is no phase transformation in various V2C7 hybrids at the hybrid ratio of 1/20; namely, all the hybrids appear as cylinder phases. As listed in Table 2, as determined from the primary peaks of the SAXS results, the (100) plane spacing (it is marked as d in Table 2) of the cylinder phase is 16.9 nm for the intrinsic V2C7 but increases to 17.2, 18.1, 18.7, and 19.0 nm after hybridization with the Ag^{+}, Cu^{2+}, Cu^{+}, and Au^{3+} ions, respectively. It indicates that significant domain swelling is induced by the addition of the Au^{3+} and Cu^{+} ions, but the swelling is moderate and insignificant in the hybrids with the Cu^{2+} and Ag^{+} ions. To further trace this distinct behavior, the hybrids with higher hybrid ratio were

Table 2. Characterization of Various Hybrids

sample	hybrid ratio	interdomain spacing (nm)	morphology	sample	hybrid ratio	interdomain spacing (nm)	morphology
V2C7	0	$d = 16.9$	C	V4C7	0	$d = 17.8$	C
Ag^+/V2C7	1/20	$d = 17.2$	C	Ag^+/V4C7	1/20	$L = 18.5$	L
Ag^+/V2C7	1/10	$d = 17.8$	C	Ag^+/V4C7	1/10	$L = 19.5$	L
Cu^{2+}/V2C7	1/20	$d = 18.1$	C	Cu^{2+}/V4C7	1/20	$L = 19.4$	L
Cu^{2+}/V2C7	1/10	$d = 19.1$	C	Cu^{2+}/V4C7	1/10	$L = 20.7$	L
Cu^+/V2C7	1/20	$d = 18.7$	C	Cu^+/V4C7	1/20	$L = 20.1$	L
Cu^+/V2C7	1/10	$d = 18.9$	C	Cu^+/V4C7	1/10	$L = 20.8$	L
Au^{3+}/V2C7	1/20	$d = 19.0$	C	Au^{3+}/V4C7	1/20	$L = 21.2$	L
Au^{3+}/V2C7	1/10	$L = 20.1$	L	Au^{3+}/V4C7	1/10	$L = 24.5$	L

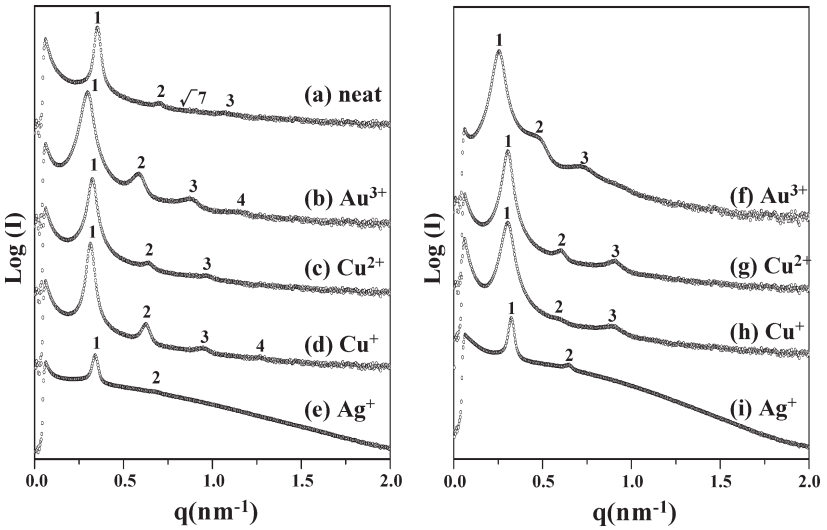

Figure 5. 1D SAXS profiles of (a) V4C7 ($f_{P4VP}^{v} = 0.38$) and its hybrids with $HAuCl_4$, $Cu(Ac)_2$, CuAc, and $AgNO_3$ at the hybrid ratios of 1/20 and 1/10 in (b)−(e) and (f)−(i), respectively.

examined. As listed in Table 2, by increasing the hybrid ratio to 1/10, the (100) plane spacing of hybrids with the Ag^+, Cu^{2+}, and Cu^+ ions change to 17.8, 19.1, and 18.9 nm, respectively.

Also, instead of cylindrical morphology, the hybrids with the Au^{3+} ions appears as lamellar morphology with the long period spacing (it is marked as L in Table 2) of 20.1 nm. Consistently, the degree of domain swelling is extremely large in the hybrids with the Au^{3+} ions so as to lead the phase transformation. By contrast, intermediate domain swelling can be found in the hybrids with the $Cu^{2+}$and Cu^+ ions. As expected, slight domain swelling can be found in the hybrids with the Ag^+ ions. In summary, the degree of domain swelling in various hybrids increases with the enhancement of association strength following the order of $Au^{3+} > Cu^{2+}$ and $Cu^+ > Ag^+$. To further examine the correlation between the association strength and the domain swelling, V4C7 ($f_{P4VP}^{v} = 0.38$) was used for hybridization. The SAXS results reflect that original cylindrical phase (Figure 5a) transfers to lamellar phase (Figure 5b−e) by the addition of Au^{3+}, Cu^{2+}, and Cu^+ ions. In contrast to the phase behavior in V2C7 hybrids, all V4C7 hybrids at a hybrid ratio of 1/20 encountered the phase transformation form cylinder to lamellae due to the close composition to that of lamellar morphology.

Further increasing the added amount of metal ions to a hybrid ratio of 1/10 leads the shifting of primary peak of the SAXS profile to lower value as shown in Figure 5f−i. Consistent with the observations in the V2C7 hybrids, the shifting of the primary peaks in the SAXS profiles (Table 2) indicates that the domain size of hybridized lamellae increases with the increase of association strength following the order of $Au^{3+} > Cu^{2+}$ and $Cu^+ > Ag^+$. The long period spacings of lamellae in the hybrids with Ag^+, Cu^{2+}, Cu^+, and Au^{3+} ions are 18.5, 19.4, 20.1, and 21.2 nm, respectively (Table 2). The results of the hybrids with higher added amounts of metal ions are also in line with the results of hybrids at a hybrid ratio of 1/20; the long period spacing increases with the increase of association strength.

According to the scattering results in Table 2, the hybridized P4VP chains tend to gain more contact area with metal ions to decrease enthalpic energy so that the driving force for the decrease of enthalpic energy is indeed correlated with the association strength. As illustrated in Figure 6, the length of hybridized P4VP chain is justified by the association strength of surrounding metal ions. In the hybrids with weak association (e.g., the Ag^+/P4VP−PCL hybrids), the enthalpic benefit from the association is insufficient to overcome the entropic penalty of P4VP chain stretching. As a result, no significant domain swelling was founded in the Ag^+/P4VP−PCL hybrids. By contrast, for the hybrids with strong association (e.g., the Au^{3+}/P4VP−PCL hybrids), the entropic penalty from P4VP chain stretching can be balanced by the enthalpic benefit from the association. Consequently, we suggest that the origin for distinct domain swelling in various hybrids may have resulted from the balance of enthalpic association and entropic chain stretching. Notably, as compared to the density of neat BCP, no significant change on the density can be traced in the hybrids (the variation in the densities of the hybrids examined is less than 0.02 g/cm^3), suggesting that high-density metal precursors give a relative high effective excluded volume so that the overall density remains invariable.

Furthermore, as observed, the introduction of the Cu^+ with single valence for hybridization gives rise to the same

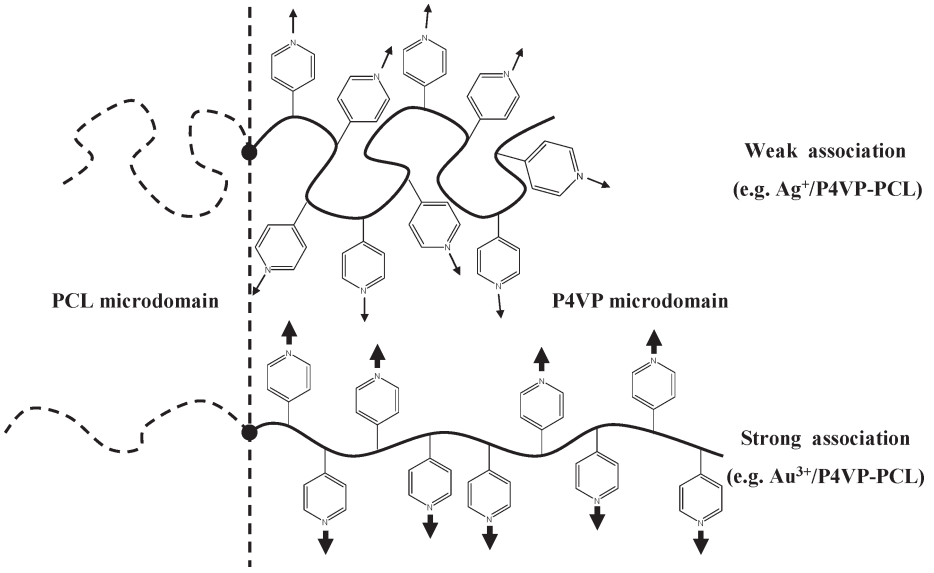

Figure 6. Schematic illustrations of the P4VP chain stretching under the weak association and strong association.

degree of domain swelling to the hybrids having the Cu^{2+} ions with two valences. In general, univalent and divalent copper ions form two and four coordination bonds with organic ligands, respectively. Accordingly, as compared to the Cu^{+}/P4VP−PCL hybrids, higher domain swelling in the Cu^{2+}/P4VP−PCL hybrids is expected. However, the association of the Cu^{2+} ions and P4VP block leads to the formation of coordination pendant group due to the existence of copper(II) acetate hydrate ($Cu(Ac)_2 \cdot xH_2O$) at which only one pyridine in the polymer chain can be associated with the divalent copper ions. By contrast, active univalent copper ions (i.e., copper(I)) tend to incorporate with one pyridine or two so as to form stable chemical state.[31] As a result, we speculate that the type of coordinated mechanism is critical to determine the degree of domain swelling so as to lead the same degree of domain swelling in the Cu^{+}/V2C7 and Cu^{2+}/V2C7 hybrids.

Phase Behavior of Au NPs/P4VP−PCL Hybrids. According to the theoretical prediction for the binding energy of metal ions or metal elements to the pyridine unit, the association strength can be effectively reduced from ionic state to element state. The predicted association strengths for various metal ions and corresponding elements follow the order of $Ag < Au < Cu < Ag^{+} < Cu^{+} < Au^{+}$.[32] On the basis of the prediction, the association strength of the metal ions with the P4VP block would be decreased by the reduction of the metal ions. For the Au^{3+}/P4VP−PCL hybrids, it is reasonable to expect a significant change in the association strength after the chemical reduction of the Au^{3+} ions to Au NPs. Figure 7a shows the TEM image of Au^{3+}/V4C7 hybrids at a hybrid ratio of 1/7 at which diffused lamellar morphology with blurred interface between the PCL and hybridized P4VP microdomains can be found. To trace the morphological evolution during the reduction, the bulk samples of the Au^{3+}/V4C7 hybrids were directly immersed into hydrazine liquid (that is, the reduction agent for the reduction of the Au^{3+} ions) for different reaction times and then dried for TEM observation. As illustrated in Figure 7b, for the sample with 1 h reaction time, the TEM image shows that randomly dispersed Au NPs with different size can be formed in addition to intrinsic lamellar morphology.

Note that there are no identified diffused boundaries; instead, well-defined interface can be observed in the Au NPs/V4C7 hybrids. Moreover, significant aggregation can be found while the reduction time further increases (results no shown). On the basis of the morphological evolution, especially the exclusion and the corresponding aggregation of the Au NPs, it is reasonable to infer that the association strength of the Au^{3+} ions with the P4VP block should be demolished by the reduction. Also, the larger Au NPs is difficult to be associated by P4VP chains so as to cause the aggregation of the Au NPs (see below for reasons).

As a result, the change on the interfacial morphology suggests that the associated P4VP chains (left) in the hybrids should be gradually released from the Au NPs (right) due to the weak association between the Au NPs and the P4VP block as illustrated in Figure 7c. Consequently, the formation of the Au NPs would give rise to the recovery of microphase-separated morphology with clear-cut boundaries and eventually return to the pristine state (i.e., cylinder phase). Similar results can be also found in the hybrids with various metal ions such as the Ag^{+} and Cu^{+} ions. Systematic studies on the phase behavior of the hybrids with various metals ions and elements are still in progress.

Particle Size Effect on Phase Behavior of Hybrids. Although the solid−liquid (i.e., polymeric bulk/hydrazine) interfacial reduction used above is convenient to trace the formation of the Au NPs, the size and the distribution of the Au NPs in the hybrids are not easy to be controlled. To well control the formation of the Au NPs, a liquid−gas interfacial reduction was carried out at which the reaction was conducted by the introduction of hydrazine vapor to the Au^{3+}/V3C5 solution. The TEM image (Figure 8a) exhibits that well-dispersed Au NPs (particle size is about 5−7 nm) can be formed through this liquid−gas interfacial reduction. The majority of the Au NPs is located near the center of P4VP microdomains (i.e., the dark regions due to RuO4 staining), which is consistent with the prediction of theoretical simulation.[18] Because of the large particle size, it is unfavorable for the Au NPs to be associated with the P4VP chains. Therefore, the formation of large Au NPs would cause the aggregation and eventually form a particle-rich phase within the P4VP microdomain. This additional microsegregation would reduce the elastic energy of the P4VP chains, but the loss of translational entropy for the particles would cause the increase in the particle-related free energy.

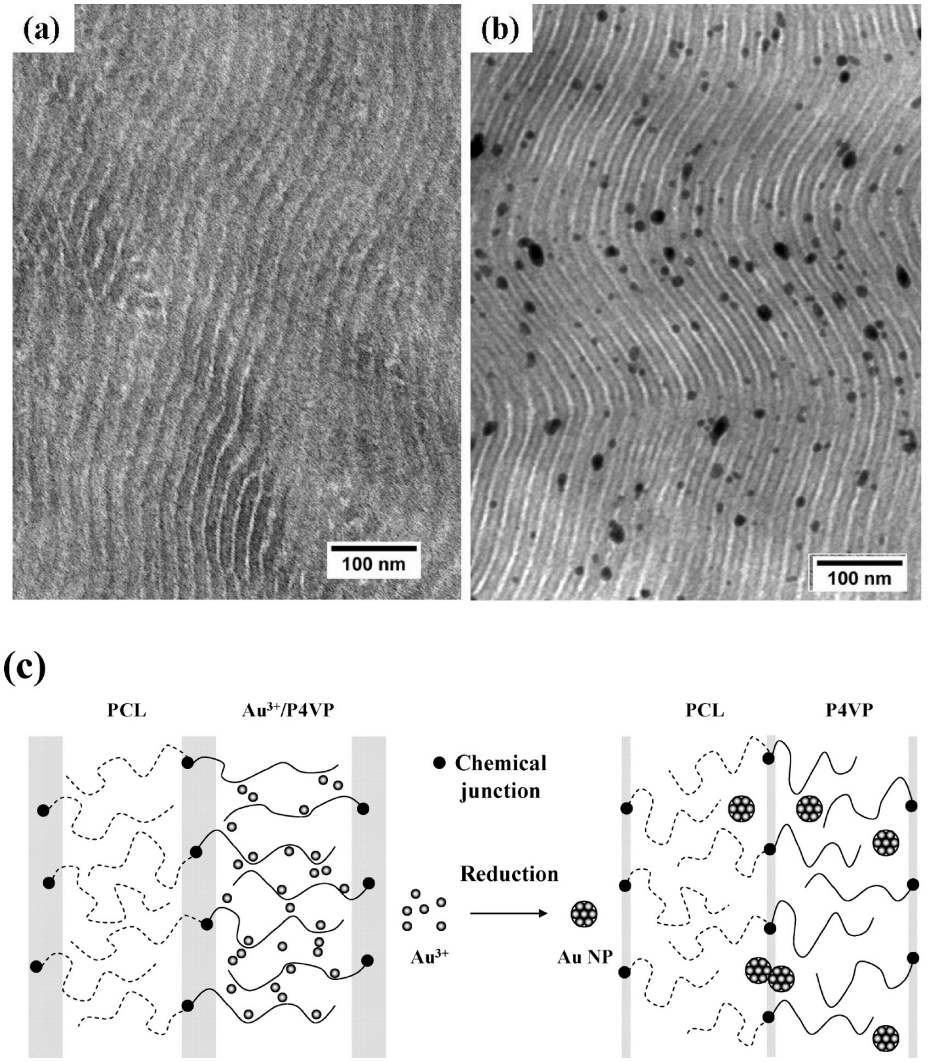

Figure 7. TEM micrographs of (a) V4C7 ($f_{P4VP}^{v} = 0.38$) hybrids with $HAuCl_4$ at a hybrid ratio of 1/7 and (b) its result after the reduction. All samples are stained by RuO_4 at which the dark region represents the P4VP microdomain and the bright region is the PCL microdomain. (c) Schematic illustration of the molecular dispositions in the Au^{3+}/V4C7 hybrid before (left) and after (right) the reduction.

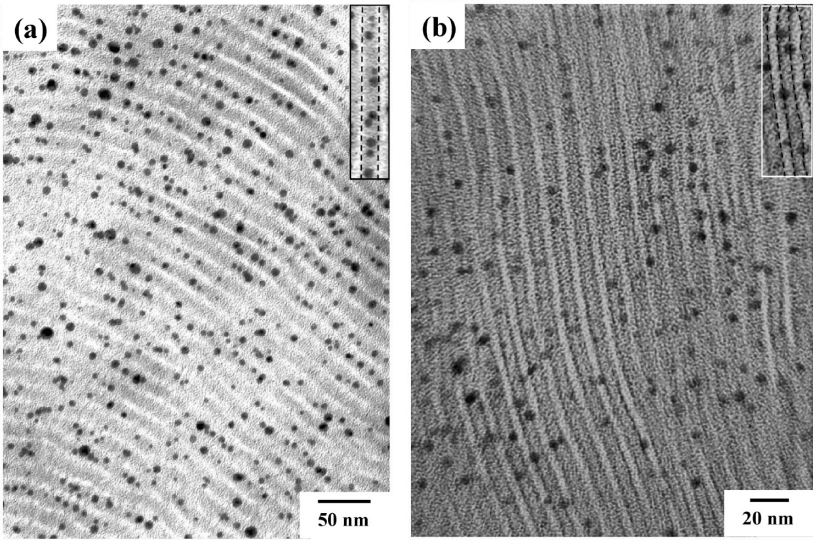

Figure 8. TEM micrographs of V3C5 ($f_{P4VP}^{v} = 0.37$) hybrids with (a) large size and (b) small size of Au NPs. The insets show that the locations of Au NPs are center-packed and edged-packed in the (a) and (b), respectively. All samples are stained by RuO_4 at which the dark region represents the P4VP microdomain and the bright region is the PCL microdomain.

The balancing of these two contributions leads to the stability of center-localized packing behavior for the Au NPs. By contrast, an almost edge-assembled morphology with the Au NPs near the interface of P4VP−PCL can be found in the hybrid with small particle size (particle size is less than 5 nm) (Figure 8b), suggesting that the Au NPs with small size prefer to be associated by P4VP microdomain. Although the concern of enthalpic penalty due to the increase of the contact area between PCL microdomain and the Au NPs is still an open question, the size of the Au NPs is indeed a critical factor to justify the accommodation of the Au NPs within the P4VP microdomain. As a result, the association effect should be also dependent upon the particle size; the larger the particle size is, the weaker the association will be.

Conclusions

In conclusion, the phase behavior of inorganic/P4VP−PCL hybrids can be significantly affected by the association of various metal species with the P4VP block. In the metal ions/P4VP−PCL hybrids, the association strength can be used as an indictor to determine the degree of P4VP chain stretching. With increasing the association strength (i.e., the P4VP chain stretching), the change in the hybrids can be effectively reflected by the domain swelling; the higher the association strength is, the higher the domain swelling will be. We speculate that the hybridized P4VP chains tend to gain more contact area with metal ions to decrease enthalpic energy so that the driving force for the decrease of enthalpic energy is indeed correlated with the association strength. Through the reduction, this association strength can be effectively diminished so as to lead the recovery of microphase-separated morphology. Furthermore, the association strength is also dependent upon the particle size; the larger the particle size is, the weaker the association will be. Consequently, the accommodation of the metal NPs within the P4VP microdomain is justified by the size of the metal NPs.

Acknowledgment. This research was supported by the National Science Council (NSC 98-2221-E-007-007) of Taiwan and Electronics Research & Service Organization, Industrial Technology Research Institute (ITRI) of Taiwan. We thank Dr. B. S. Hsiao of the Chemistry Department, State University of New York at Stony Brook, and Dr. U. S. Jeng and Dr. Y. S. Sun of the National Synchrotron Radiation Research Center (NSRRC) for their help in synchrotron SAXS experiments.

Supporting Information Available: TEM micrographs of V2C7 (Figure S1). This material is available free of charge via the Internet at http://pubs.acs.org.

References and Notes

(1) Spatz, J. P.; Roescher, A.; Moller, M. *Adv. Mater.* **1996**, *8*, 337.
(2) Templin, M.; Franck, A.; Chesne, A. D.; Leist, H.; Zhang, Y.; Ulrich, R.; Schadler, V.; Wiesner, U. *Science* **1997**, *278*, 1795.
(3) Forster, S.; Antonietti, M. *Adv. Mater.* **1998**, *10*, 195.
(4) Thurn-Albrecht, T.; Schotter, J.; Kastle, G. A.; Emley, N.; Shibauchi, T.; krusin-Elbaum, L.; Guarini, K.; Black, C. T.; Tuominen, M. T.; Russell, T. P. *Science* **2000**, *290*, 2126.
(5) Lopes, W. A.; Jaeger, M. *Nature* **2001**, *414*, 735.
(6) Bockstaller, M. R.; Kolb, R.; Thomas, E. L. *Adv. Mater.* **2001**, *13*, 1783.
(7) Ribbe, A. E.; Okumura, A.; Matsushige, K.; Hashimoto, T. *Macromolecules* **2001**, *34*, 8239.
(8) Sohn, B. H.; Seo, B. H. *Chem. Mater.* **2001**, *13*, 1752.
(9) Boontongkong, Y.; Cohen, R. E. *Macromolecules* **2002**, *35*, 3647.
(10) Yeh, S. W.; Wei, K. H.; Sun, Y. S.; Jeng, U. S.; Liang, K. S. *Macromolecules* **2003**, *36*, 7903.
(11) Bockstaller, M. R.; Thomas, E. L. *Phys. Rev. Lett.* **2004**, *93*, 166106.
(12) Li, H.; Eddaoudi, M.; O'keeffe, M.; Yaghi, O. M. *Nature* **1999**, *402*, 276.
(13) He, Y.; Lodge, T. P. *Macromolecules* **2008**, *41*, 167.
(14) Huh, J.; Ginzburg, V. V.; Balazs, A. C. *Macromolecules* **2000**, *33*, 8085.
(15) Hashimoto, T.; Tanaka, H.; Hasegawa, H. *Macromolecules* **1990**, *23*, 4378.
(16) Lodge, T. P.; Pudil, B.; Hanley, K. J. *Macromolecules* **2002**, *35*, 4707.
(17) Ginzburg, V. V.; Gibbons, C.; Qiu, F.; Peng, G.; Balazs, A. C. *Macromolecules* **2000**, *33*, 6140.
(18) Thompson, R. B.; Ginzburg, V. V.; Matsen, M. W.; Balazs, A. C. *Science* **2001**, *292*, 2469.
(19) Bockstaller, M. R.; Lapetnikov, Y.; Margel, S.; Thomas, E. L. *J. Am. Chem. Soc.* **2003**, *125*, 5276.
(20) Kim, B, J.; Chiu, J. J.; Yi, G. R.; Pine, D. J.; Kramer, E. J. *Adv. Mater.* **2005**, *17*, 2618.
(21) Epps, T. H.; Bailey, T. S.; Pham, H. D.; Bates, F. S. *Chem. Mater.* **2002**, *14*, 1706.
(22) Sidorov, S. N.; Bronstein, L. M.; Kabachii, Y. A.; Valetsky, P. M.; Soo, P. L.; Maysinger, D.; Eisenberg, A. *Langmuir* **2004**, *20*, 3543.
(23) Lee, D. H.; Kim, H. Y.; kim, J. K.; Huh, J.; Ryu, D. Y. *Macromolecules* **2006**, *39*, 2027.
(24) Lee, D. H.; Han, S. H.; Joo, W.; Kim, J. K.; Huh, J. *Macromolecules* **2008**, *41*, 2577.
(25) He, Y.; Li, Z.; Simore, P.; Lodge, T. P. *J. Am. Chem. Soc.* **2006**, *128*, 2745.
(26) Simore, P.; Lodge, T. P. *Macromolecules* **2008**, *41*, 1753.
(27) Wang, J. P.; Chen, W.; Roy, C.; Sievert, J. D.; Russell, T. P. *Macromolecules* **2008**, *41*, 963.
(28) Wang, J. P.; Chen, W.; Russell, T. P. *Macromolecules* **2008**, *41*, 4904.
(29) Ho, R. M.; Lin, T.; Jhong, M. R.; Chung, T. M.; Ko, B. T.; Chen, Y. C. *Macromolecules* **2005**, *38*, 8607.
(30) Lin, T.; Ho, R. M.; Ho, J. C. *Macromolecules* **2009**, *42*, 742.
(31) Belfiore, L. A.; Mccurdie, M. P. *J. Polym. Sci., Polym. Chem.* **1994**, *33*, 105.
(32) Wu, D. Y.; Ren, B.; Jiang, Y. X.; Xu, X.; Tian, Z. Q. *J. Phys. Chem. A* **2002**, *106*, 9042.